Supplementary Information

Colloidal Behavior of Cellulose Nanocrystals Grafted with Poly(2-alkyl-2-oxazoline)s

Cony Gauche [a], Maria Isabel Felisberti [a*]

[a] Institute of Chemistry, University of Campinas, PO Box 6154, 13084-971, Campinas – SP, Brazil.

Corresponding author: Maria Isabel Felisberti

Address: Institue of Chemistry, Josué de Castro, 126 - Cidade Universitária, Campinas - SP, 13083-861

Email: misabel@unicamp.br

Tel.: +55 19 3721-3419

Fax: +55 19 3521-3023

Summary

CNC's surface modification

The CNC's surface modification by TEMPO-mediated oxidation was completely characterized concerning its physicochemical properties in order to guarantee inner characteristics of pristine crystals. The exact determination of sample degree of oxidation (DO) is decisive for the next step, wherein polyoxazoline chains will be grafted onto the CNCs surface via peptidic coupling reaction and different approaches were explored to ensure DO accuracy. FTIR and conductometry analyses were used for this determination (Figure S1, Table S1).

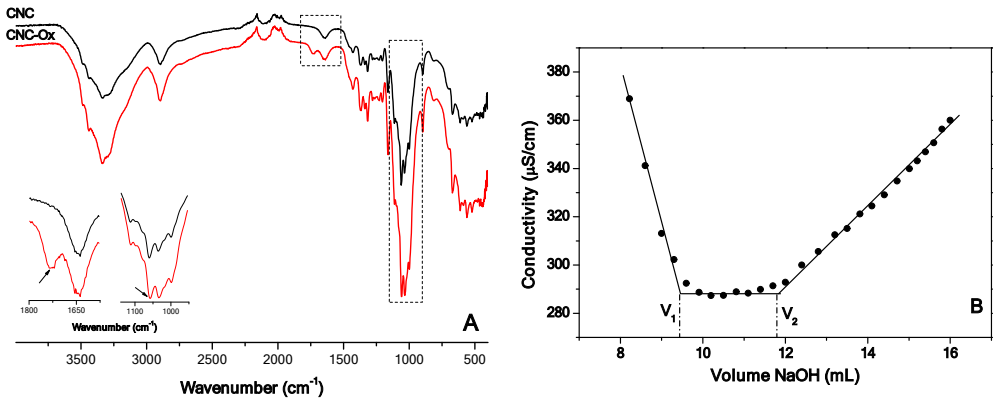

Figure S1. (**A**) FTIR spectra for pristine CNC and oxidized CNC and (**B**) conductimetric titration curves of oxidized CNC.

Table S1. Characteristics of pristine and oxidized CNCs: DO (degree of oxidation), C6 (signal area ratio at 63/65 ppm from ^{13}C NMR), ξ-potential (mV), T_{onset}°C (temperature of initial degradation), $T_{máx}$°C (temperature of maximum degradation rate), CI (crystallinity index), L (length), d (diameter), L/d (aspect ratio).

Sample	DO[1]	DO[2]	C6	ξ	T_{onset}°C	$T_{máx}$°C	CI (%)[3]	L[4] (nm)	D[4] (nm)	L/d
CNC	-	-	2.58	-63.9	205 °C	302 °C	83	105±35	4.7±1.1	22
Oxidized CNC	0.049	0.051	1.26	-71.6	200 °C	302 °C	76	101±20	5.2±1.1	19

* Determined by: [1] conductometric titration, [2]FTIR, [3]DRX, [4]AFM.

Owing to oxidation, the presence of a signal at 173.8 ppm in the ^{13}C NMR spectrum (Figure S2) corresponding to the carboxyl groups introduced onto CNC's surface confirms the hydroxyls modification by TEMPO reaction. A decrease of the signals area ratio $C6_{amorphous}$ / $C6_{cristalline}$ (63 ppm / 65 ppm) was observed due to the decrease of primary hydroxyl groups on the surface and in amorphous domains, since it is known that the oxidation occurs mostly in the disordered regions of the sample.[1]

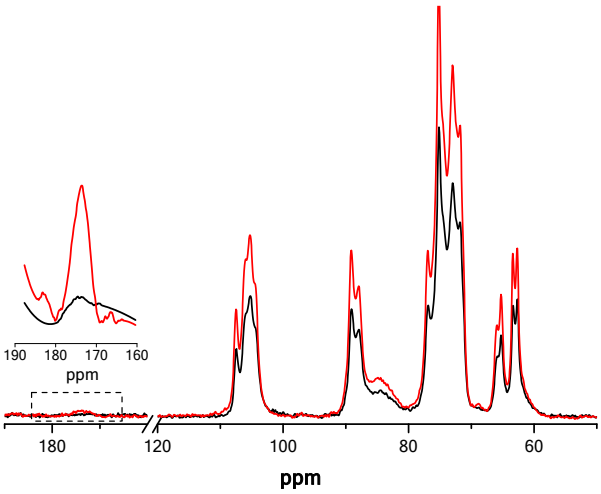

Figure S2. ^{13}C NMR spectra for pristine CNC (black line) and oxidized CNC (red line).

Pristine CNCs are highly crystalline and have been used as reinforcing agents for innumerous polymer matrices.[2] The diffractograms in Figure S3 show the $(1\bar{1}0)$, (110), (002) and (040) reflections, which corresponds to cellulose I diffraction peaks. Besides, cellulose II is also present as one can observe in the CNC pattern at 2θ = 12.5, 20.1, 22.7 and 34.4.[3,4] The coexistence of cellulose I and cellulose II in CNCs is well known in commercial samples, and probably arises from the use of harsh conditions during particle obtainment by acid hydrolysis (or post-hydrolysis neutralization), causing the transformation of cellulose I into cellulose II within the crystalline domains.[5]

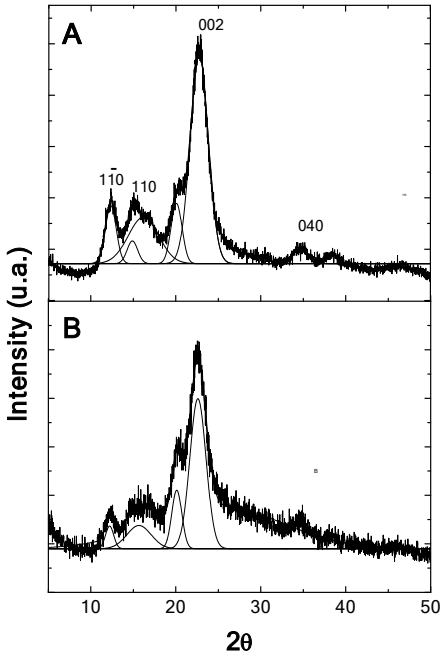

Figure S3. XRD diffraction patterns for pristine (**A**) CNCs and oxidized (**B**) CNCs.

Pristine CNCs present a needle-like structure with an average length (L) of 105 ± 35 nm, a diameter (d) of 4.7 ± 1.1 nm (height measured from z-scale), and a resultant aspect ratio of 22 (based on 100 measurements from 5 micrographs) (Table S1).

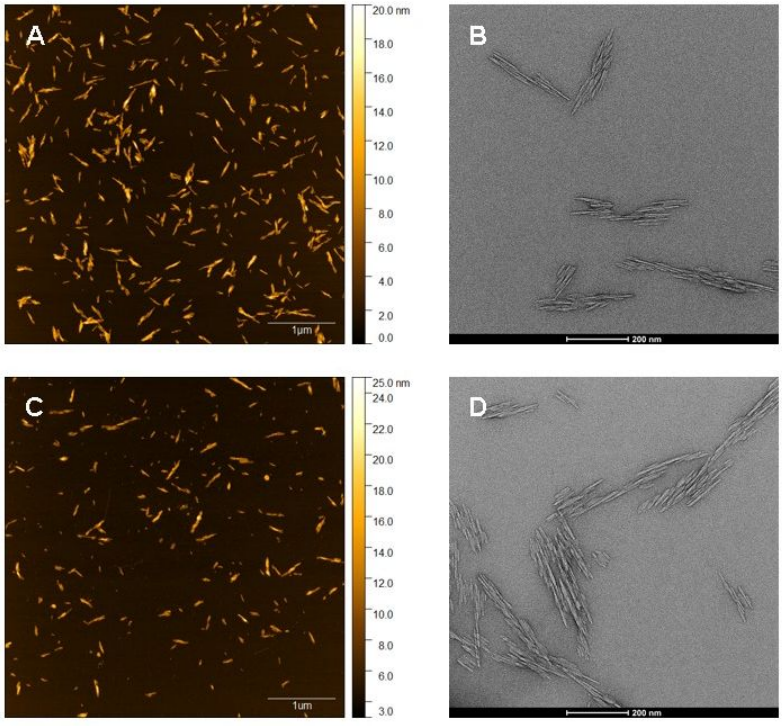

Figure S4. Images of pristine (**A**)-(**B**) CNCs and oxidized (**C**)-(**D**) CNCs obtained by (**A and C**) atomic force microscopy and (**B and D**) transmission electron microscopy.

It is worth mentioning that crystals' diameters calculated from TEM images is according to those obtained from z-scale, from AFM micrographs. The CNC used in this work were provided by the University of Maine, and the aspect ratio value obtained was consistent with the values reported in the literature by other research groups using the same source.[6] The micrographs shown at Figure S4 confirm that TEMPO-mediated oxidation preserves the integrity and shape of the CNCs by introducing carboxylate groups at their surface. Needle-like structures with an average length (L) of 101 ± 20 nm, a diameter of 5.2 ± 1.1 nm and a resultant aspect ratio of 19 were observed to oxidized CNCs, meaning that the degradation of the crystals is negligible during oxidation reaction.[7]

Synthesis of Poly(2-alkyl-2-oxazoline)s

Poly(2-ethyl-2-oxazoline) (PEtOx) polymerization targeting a DP of 100 unimers was performed at 120 °C in acetonitrile in different reaction times: 1h, 3h, 16h and 24h. After 1 hour, one can assume the polymerization reaction is completed (> 95% of yield). Increasing the reaction time, yellowish polymers are obtained (Figure S5A) as a consequence of chain transfer reactions.[8] Figure S5 summarizes homopolymers molar mass distributions determined by GPC. Chromatograms obtained from refraction index detector (Figure S5B) for PEtOx after 16h and 24h of reaction showed a defined shoulder at shorter retention times, indicative of bimodal molar mass distribution and the presence of high molar mass polymers. On the other hand, when UV detector is applied (Figure S5C), the intensity of this shoulder increases as longer is the reaction time (Figure S5D), suggesting the presence of chromophores in the polymer chains responsible for UV absorption (Figure S5E). Moreover, a slight bathochromic shift occurs by increasing reaction time, from 322 nm (1h) to 328 nm (24 h).

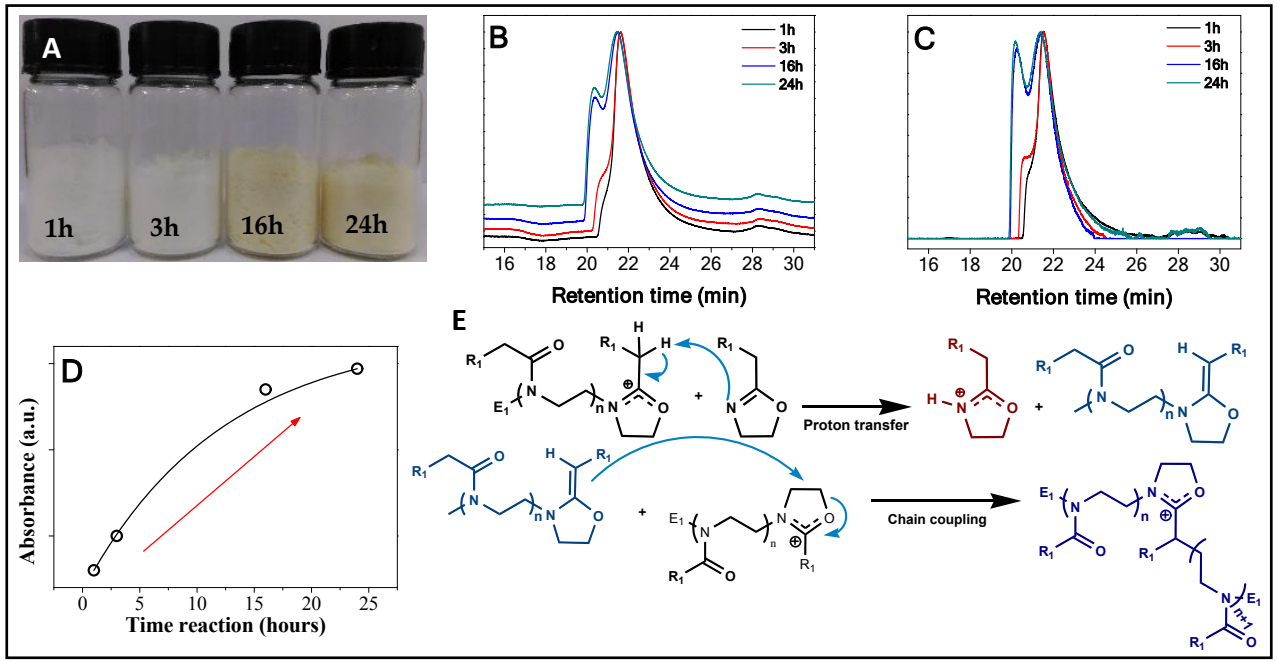

Figure S5. (**A**) Illustrative image of polymer color changes as a function of time reaction. GPC chromatograms for PEtOx: (**B**) IR and (**C**) UV detectors. (**D**) Maximum of absorbance values (322 – 328 nm) of PEtOx aqueous solution (20 mg mL^{-1}). (**E**) Mechanism of chain transfer reaction, adapted from ref 8.

Table S2. Molar mass of poly(2-ethyl-2-oxazoline)s determined by GPC and ^{1}H NMR, yield over reaction time and thermal properties in bulk and aqueous solution.

Target polymer	Polymer	Reaction time (h)	Yield (%)	M_n (^{1}H NMR)	M_n (GPC)	M_w (GPC)	Đ	T_{onset}°C	$T_{máx}$°C	T_g	LCST*
$PEtOx_{100}$	$PEtOx_{106}$	1	96	5.000	10.604	12.831	1,20	344	421	54	87
$PEtOx_{100}$	$PEtOx_{105}$	3	95	7.000	10.545	11.916	1,13	342	417	56	85
$PEtOx_{100}$	$PEtOx_{123}$	16	95	6.100	12.376	14.480	1,17	342	426	45	84
$PEtOx_{100}$	$PEtOx_{133}$	24	97	5.900	13.379	14984	1,12	338	411	40	82

M_n: number average molar mass, M_w: weight average molar mass, Đ: polydispersity index. T_{onset}°C : initial thermal degradation at the point of 5 % degradation. $T_{máx}$°C : temperature of maximum thermal degradation. T_g : glass transition. LCST : lower critical solubilization temperature

* 20 mg mL^{-1} aqueous solution

^{1}H NMR was also used to calculate molar masses of PEtOx and values estimated by NMR were remarkable lesser than those calculated by GPC (Table S2). The molar mass determined by ^{1}H NMR was estimated based on the integral ratios between 3.3 – 3.7 ppm (-CH_2- of backbone) and 2.7 ppm (-CH_3 of initiator) (Figure S8). Results determined by GPC, in its turn, were recorded from a multidetector system using an absolute pattern of polystyrene for calibration. These differences could be related to possible polymer aggregation in aqueous solution as concluded by Chen et al. (1994)[9] from static light scattering (SLS).

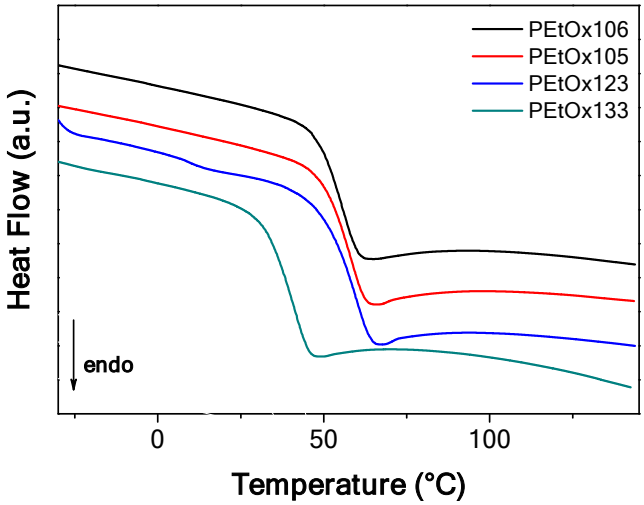

Figure S6. DSC second heating scan at 20 °C min^{-1} for P(EtOx)s.

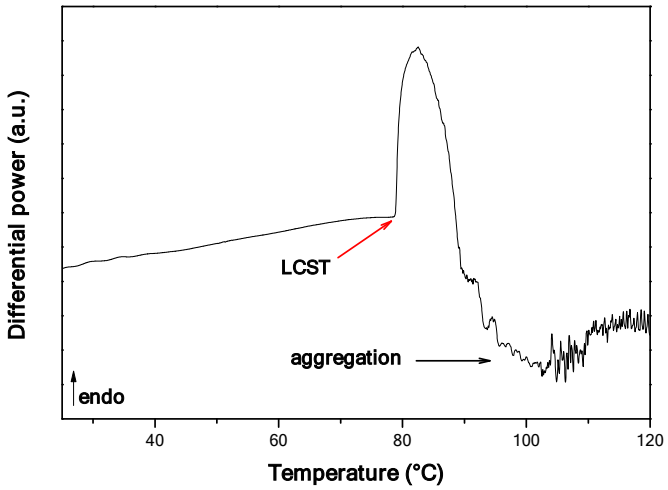

Figure S7. HSDSC first heating scan at 1 °C min^{-1} for $P(EtOx)_{106}$ aqueous solution (20 mg mL^{-1}).

After the maximum (Figure S7), the curve decreases and do not return to the base line. The same behavior was observed for thermoresponsive poly(diethylene oxide) methyl ether methacrylate.[10] Proteins have shown similar response, and this effect suggest protein aggregation, followed by precipitation of the protein.[11]

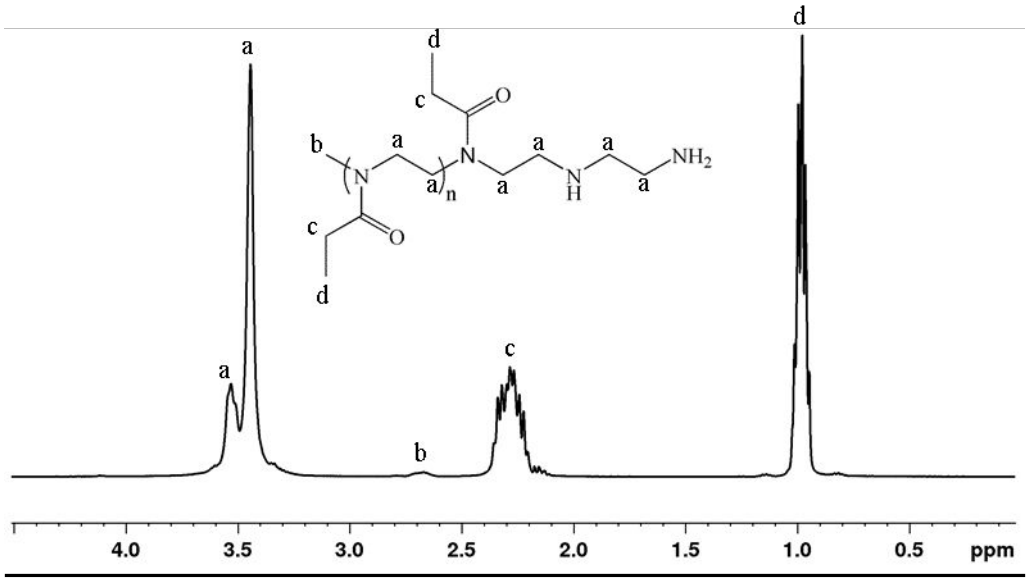

Figure S8. ^{1}H RMN spectrum for $PEtOx_{106}$ in D_2O.

PEtOx was obtained with a molar mass of 10.6 kDa and dispersity of Đ = 1.20, determined by GPC in chloroform.

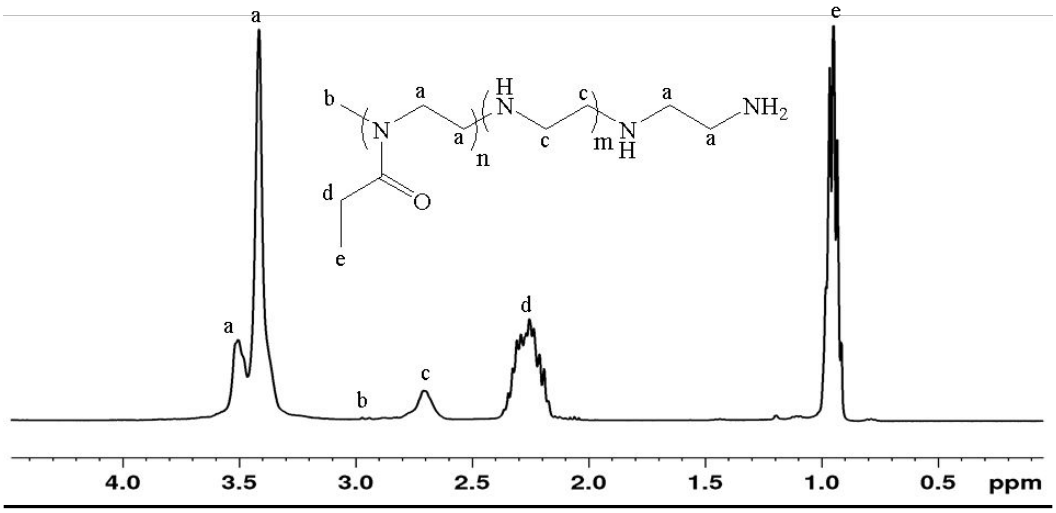

Figure S9. ^{1}H RMN spectrum for P(EtOx-*s*-Ei) in D_2O.

Hydrolysis degree was calculated from the ratio between CH_2 protons integral from the backbone of ethylene imine monomer (Hc) over the one from ethyl oxazoline monomer (Ha). Statistical copolymers were obtained with a partial hydrolysis degree of 5 and 10 %, named as $P(EtOx_{95}\text{-}s\text{-}Ei_5)$ and $P(EtOx_{90}\text{-}s\text{-}Ei_{10})$.

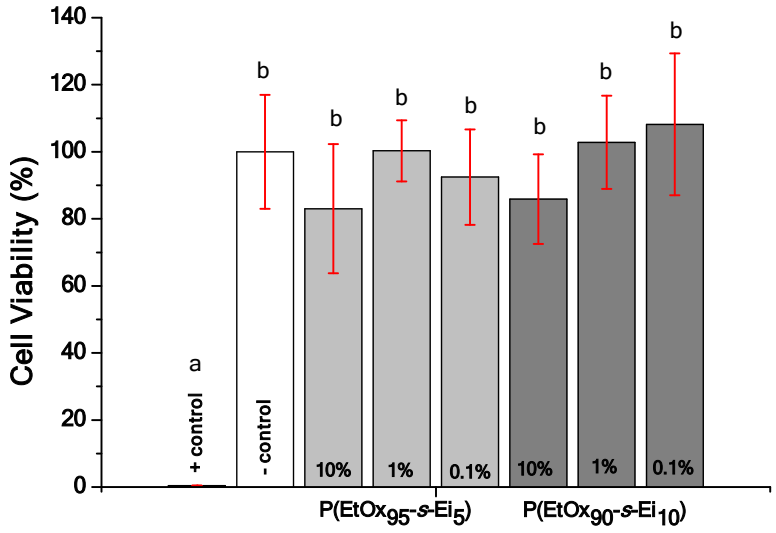

Figure S10. Cell viability determined by MTS assay for P(EtOx-*s*-Ei)s after 24 hours incubation with fibroblasts cell line NIH 3T3 with dispersions concentration of 0.1, 1 and 10 wt %. *Columns followed by the same letters do not differ significantly by the Tukey test ($p < 0.05$).

POx grafting onto CNC surfaces

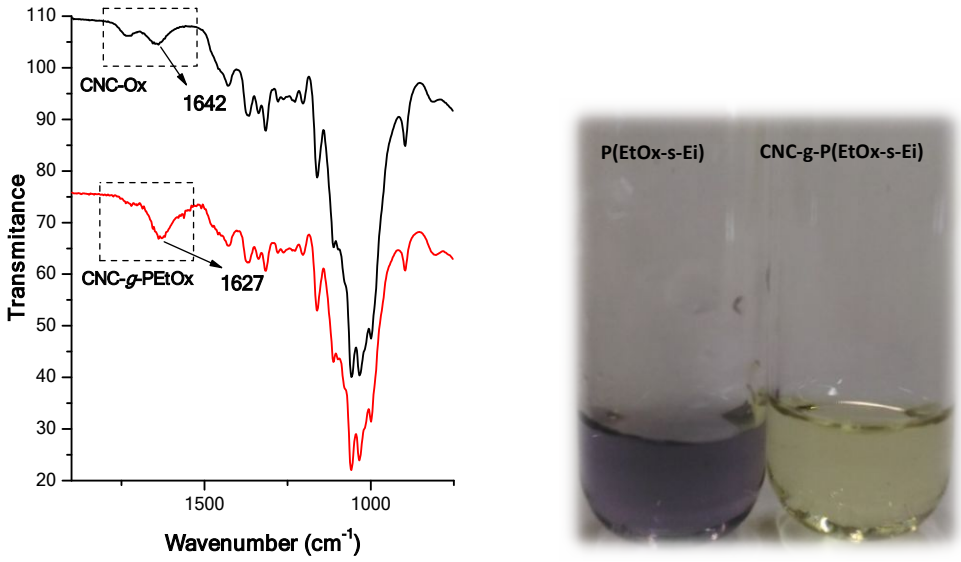

Figure S11. **Left** – FTIR spectra for TEMPO oxidized CNCs and after PEtOx grafting onto CNCs surface. **Right** – Ninhydrin test (purple color indicates the presence of primary amines in solution – free polymers; yellow color indicates the lack of primary amines – grafted polymers onto crystals' surfaces).

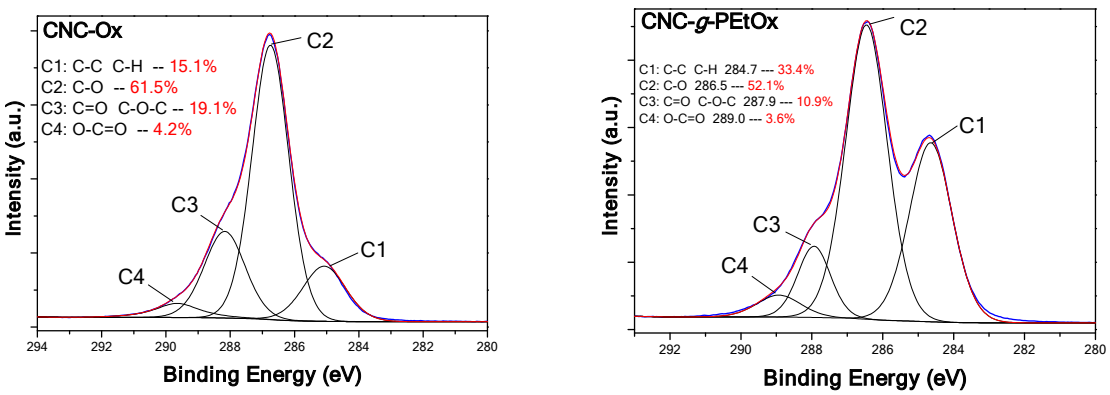

Figure S12. C1s XPS binding energy for TEMPO oxidized CNCs and CNC-*g*-PEtOx.

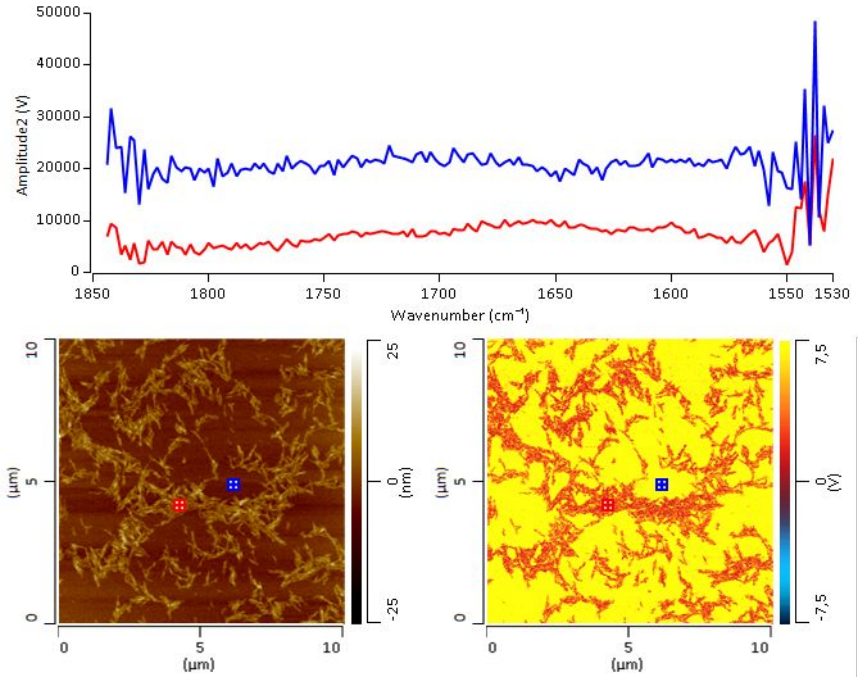

Figure S13. Atomic force microscopy with infrared spectroscopy for pristine CNCs.

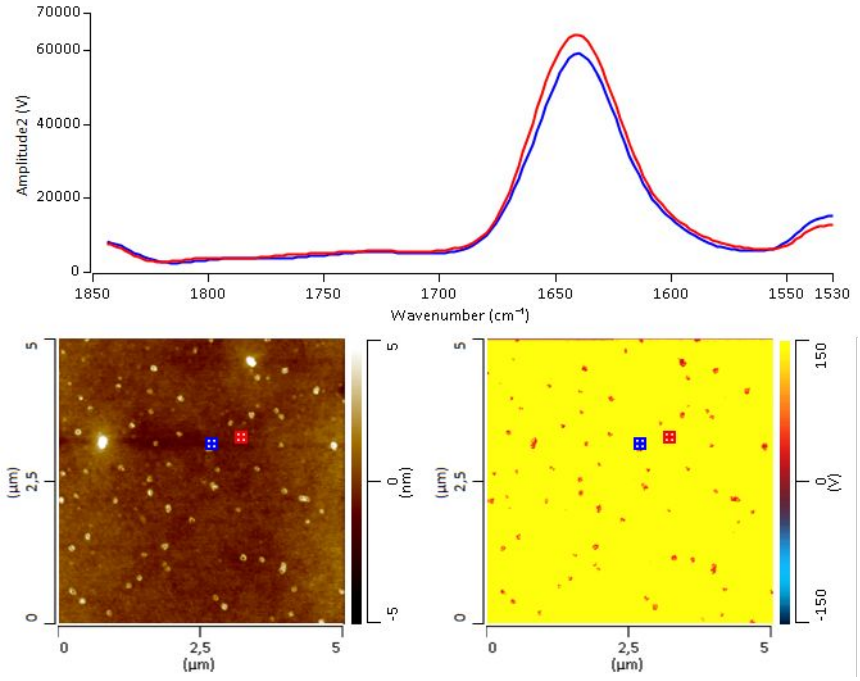

Figure S14. Atomic force microscopy with infrared spectroscopy for PEtOx (control).

Thermal properties of CNC-g-POx

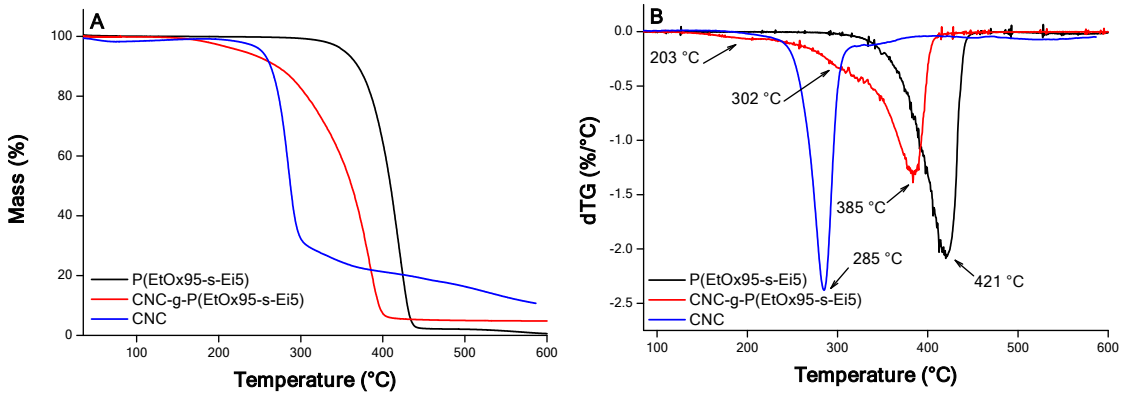

Figure S15. (**A**) TGA and (**B**) dTGA curves for $P(EtOx_{95}\text{-}s\text{-}Ei_5)_{100}$, CNC-*g*- $P(EtOx_{95}\text{-}s\text{-}Ei_5)_{100}$ and pristine CNC.

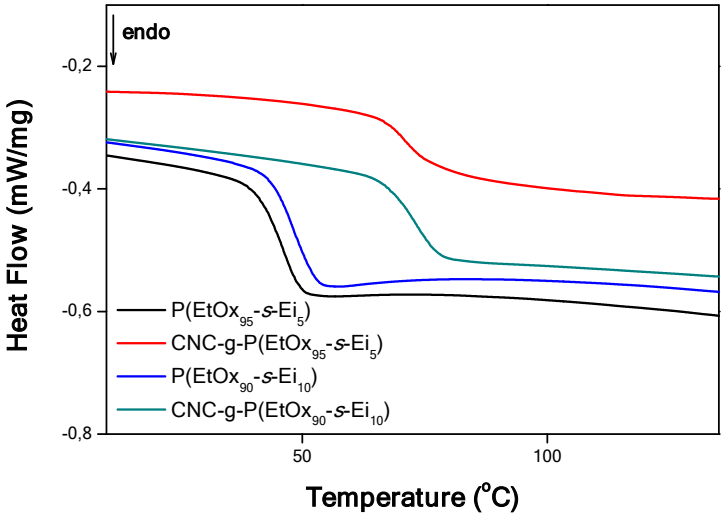

Figure S16. DSC second heating scan at 20 °C min^{-1} of P(EtOx-*s*-Ei)s and CNC-*g*-P(EtOx-*s*-Ei)s.

Cytotoxicity in vitro assay

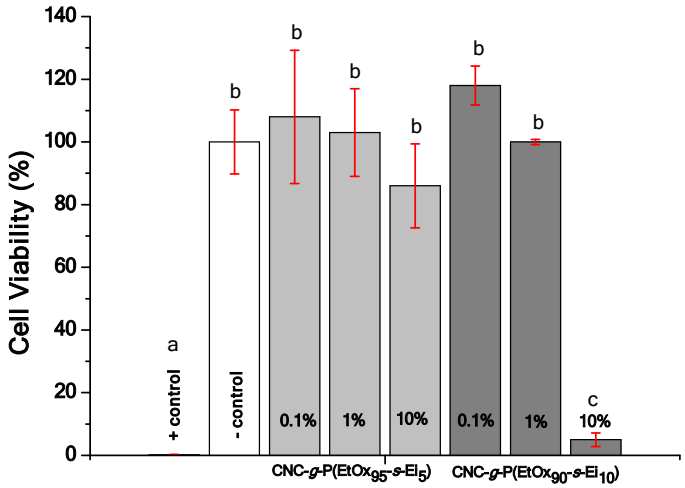

Figure S17. Cell viability determined by MTS assay for CNC-*g*- P(EtOx-*s*-Ei)s after 24 hours incubation with fibroblasts cell line NIH 3T3 with dispersions concentration of 0.1, 1 and 10 wt %. *Columns followed by the same letters do not differ significantly by the Tukey test ($p < 0.05$).

CNC-g-POx particles dispersion

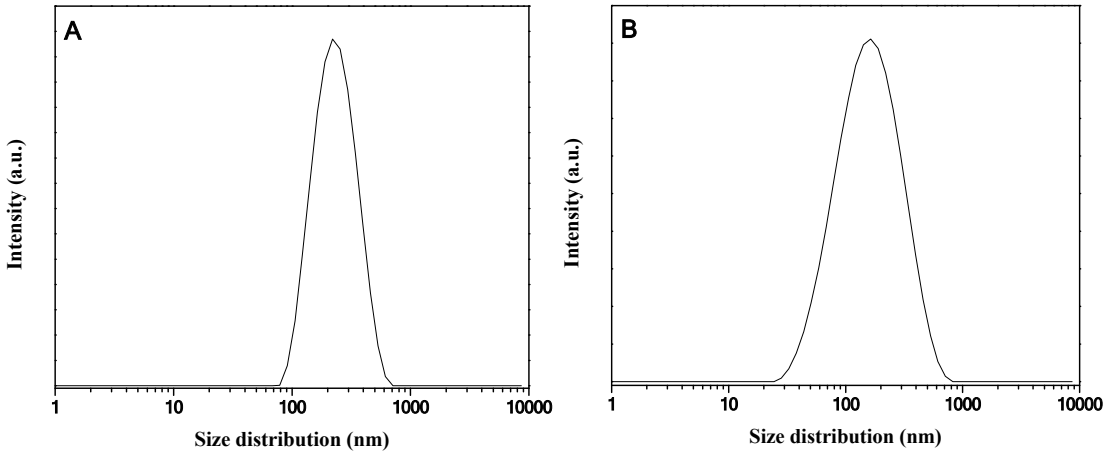

Figure S18. Size distribution for never-dried (**A**) pristine CNCs, (**B**) CNC + CNC-*g*-P($EtOx_{95}$-*s*-Ei_5) (10:1 w/w) at 0.01 wt %.

Rheological properties

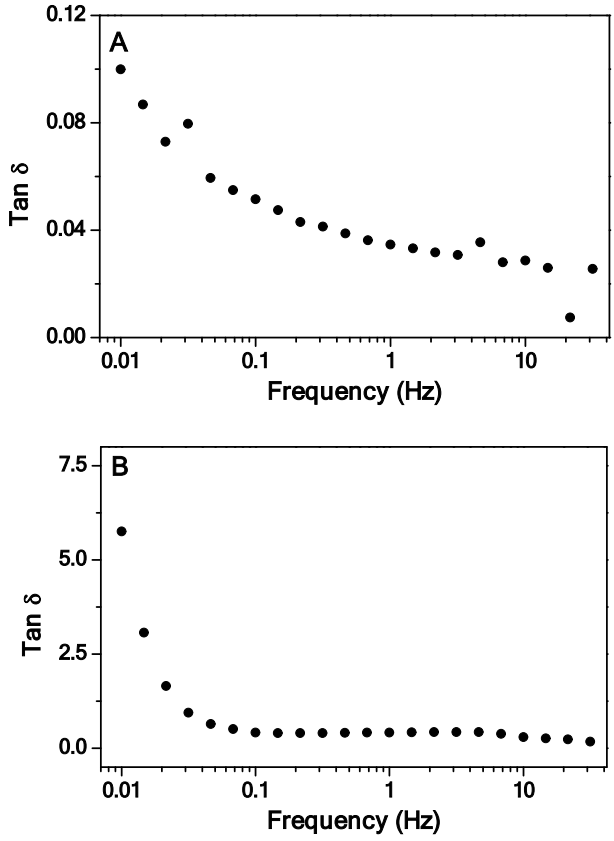

Figure S19. Tan δ values for (**A**) CNCs, (**B**) CNC + CNC-*g*-P($EtOx_{95}$-*s*-Ei_5) (10:1 w/w) dispersions at CNC concentration of 5 wt %.

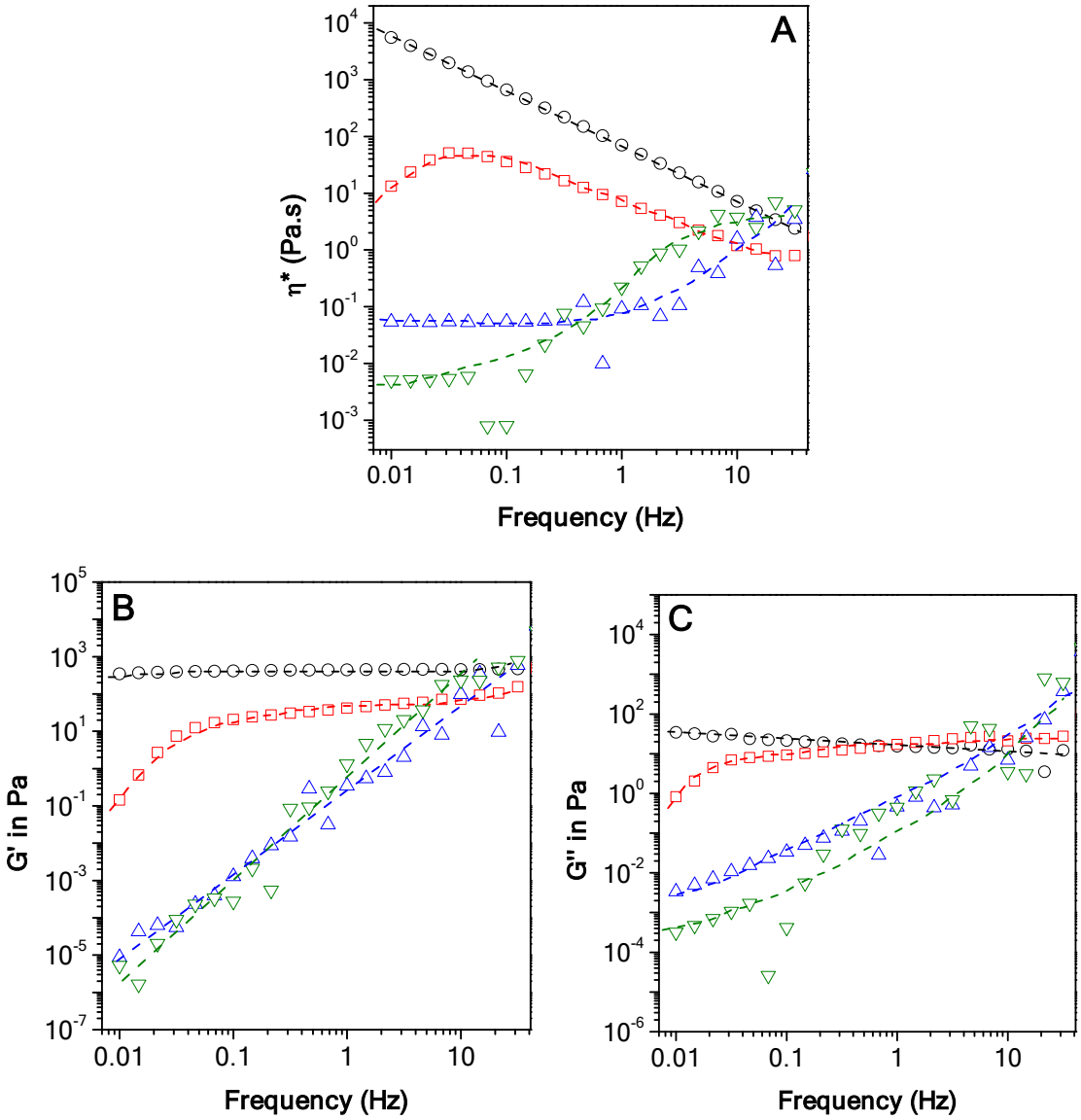

Figure S20. (**A**) Complex viscosity, (**B**) storage (G') and (**C**) loss (G'') moduli as a function of oscillatory frequency for pristine CNC dispersion (○) CNC dispersion with 10 wt % CNC-*g*-P(EtOx$_{95}$-*s*-Ei$_5$) (□), CNC dispersion with 10 wt % CNC-*g*-P(EtOx$_{95}$-*s*-Ei$_5$) dispersed after freeze-drying (Δ) and CNC-*g*-P(EtOx$_{95}$-*s*-Ei$_5$) dispersion (∇), at a CNC final concentration of 5 wt %. * Dash dot are just a guide to the eyes.

References

[1] Montanari, S.; Roumani, M.; Heux, L.; Vignon, M. R. Topochemistry of Carboxylated Cellulose Nanocrystals Resulting from TEMPO-Mediated Oxidation. *Biomacromolecules*, **2005**, 38, 1665-1671.

[2] Kargarzadeh, H.; Huang, J.; Lin, N.; Ahmad, I.; Mariano, M.; Dufresne, A.; Thomas, S. Gałęski, A. Recent developments in nanocellulose-based biodegradable polymers, thermoplastic polymers, and porous nanocomposites. *Prog. Polym. Sci*, **2018**, 87, 197-227.

[3] Driemeier, C.; Calligaris, G. Theoretical and experimental developments for accurate determination of crystallinity of cellulose I materials. *J. Appl. Crystallogr.*, **2010**, 44, 184–192.

[4] Yang, D.; Peng, X.-W.; Zhong, L.-X.; Cao, X.-F.; Chen, W.; Sun, R.-C. Effects of pretreatments on crystalline properties and morphology of cellulose nanocrystals. *Cellulose*, **2013**, 20, 2427–2437.

[5] Neto, W.P.F.; Putaux, J.-L.; Mariano, M.; Ogawa, Y.; Otaguro, H.; Pasquinia, D.; Dufresne, A. Comprehensive morphological and structural investigation of cellulose I and II nanocrystals prepared by sulphuric acid hydrolysis. *RSC Adv.*, **2016**, 6, 76017-76027.

[6] M. Mariano, C. Chirat, N.E. Kissi, A. Dufresne, Impact of Cellulose Nanocrystal Aspect Ratio on Crystallization and Reinforcement of Poly(butylene adipate-co-terephthalate). *J. Polym. Sci. B*, 54 (2016), 2284-2297.

[7] Fraschini, C.; Chauve, G.; Bouchard, J. TEMPO-mediated surface oxidation of cellulose nanocrystals (CNCs). *Cellulose*, **2017**, 24, 2775-2790.

[8] Warakomski, J. M.; Thill, B. P. Evidence for long chain branching in polyethyloxazoline. *J. Polym. Sci. A*, 1990, 28, 3551-3563.

[9] Chen, C. H.; Wilson, J.; Chen, W.; Davis, R. M.; Riffle, J. S. A light-scattering study of poly(2-alkyl-2oxazoline)s: effect of temperature and solvent type. *Polymer*, **1994**, 5, 3587-3591.

[10] Brinatti, C.; Akhlaghi, S. P.; Pires-Oliveira, R.; Bernardinelli, O. D.; Berry, R. M.; Tam, K. C.; Loh, W. Controlled coagulation and redispersion of thermoresponsive poly(diethylene oxide) methyl ether methacrylate grafted cellulose nanocrystals. *J. Colloid Interface Sci*, **2019**, 538, 51-61.

[11] Fessas, D.; Staiano, M.; Barbiroli, A.; Marabotti, A.; Schiraldi, A.; Varriale, A.; Rossi, M.; D'Auria, S. Molecular Adaptation Strategies to High Temperature and Thermal Denaturation Mechanism of the D-Trehalose/D-Maltose-Binding Protein From the Hyperthermophilic Archaeon *Thermococcus litoralis*. *Proteins: Struct. Funct. Bioinf.,* **2007**, 67, 1002-1009.